Electronic Supplementary Information (ESI)

Saloplastics as multiresponsive ion exchange reservoirs and catalyst support

CONTENT

Fig. S15: Copper molality in dry PMAA/PAH COPECs, measured by ICP, before and after annealing.

Fig. S16: XRD of annealed PMAA/PAH COPECs.

Fig. S17: Elemental mapping (EDX) of incubated PMAA/PAH COPECs after annealing.

Fig. S18: Evolution of the average diameter of copper NPs in function of incubation time of PMAA/PAH COPECs after annealing.

Fig. S19: Size distribution of copper nanoparticles in PMAA/PAH COPECs after thermal annealing.

Fig. S20: TGA analysis of PMAA/PAH COPEC under air, after annealing at 500 °C.

Fig. S21: XRD of annealed PMAA/PAH COPECs before and after being used as catalyst.

Fig. S22: Elemental mapping of incubated copper-loaded PMAA/PAH COPECs after a catalysis cycle.

Fig. S23: Conversion rate (%) of CO oxidation in function of contact time of annealed COPEC previously incubated for 300 min during the catalysis cycle.

Fig. S24: Conversion rate normalized by the copper content (%.mg^{-1}) of CO oxidation in function of contact time of annealed COPEC and commercial copper nano-

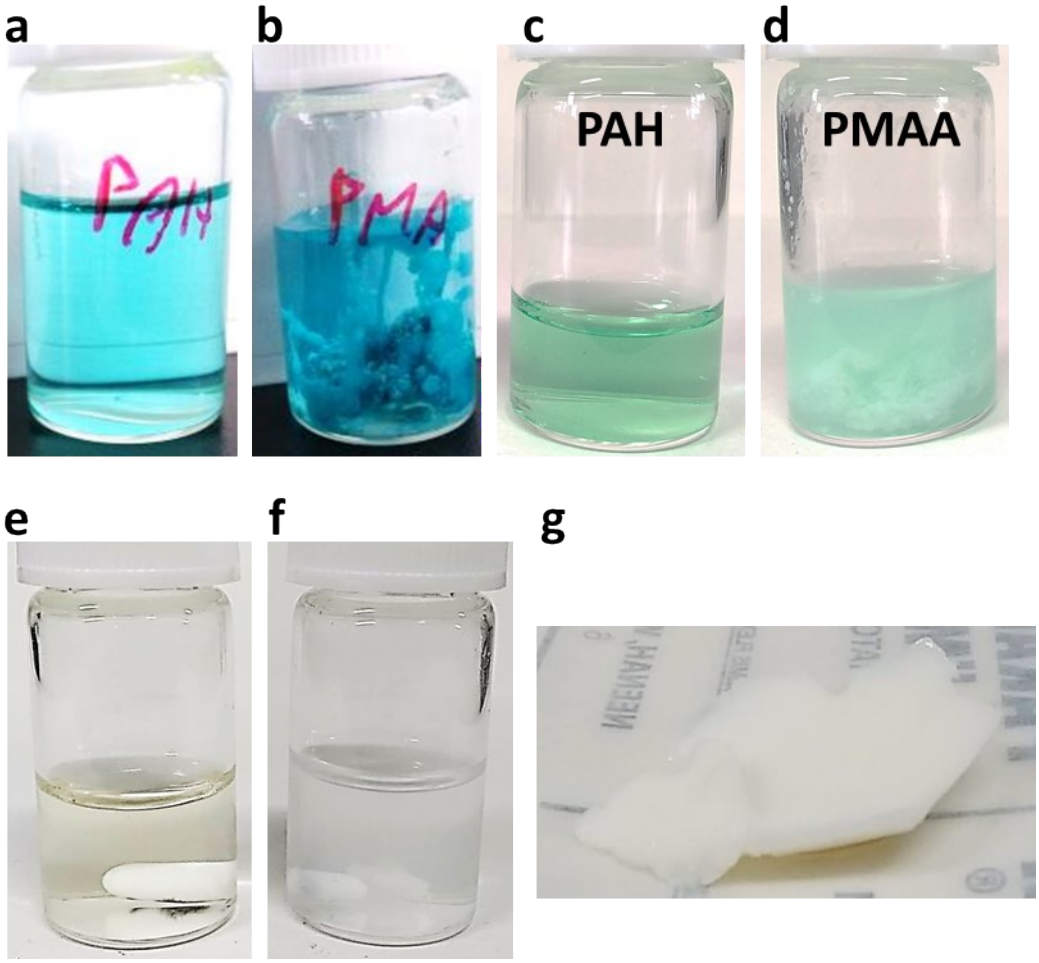

Fig. S1: Aspect of PAH and PMAA solutions concentrated at 0.3 M with respect to their monomer units in 0.2M solutions of $CuCl_2$ (a,b), $NiCl_2$ (c,d), and $MgCl_2$ (e,f). COPEC obtained by mixing PAH and PMAA solutions in presence of $MgCl_2$ (g).

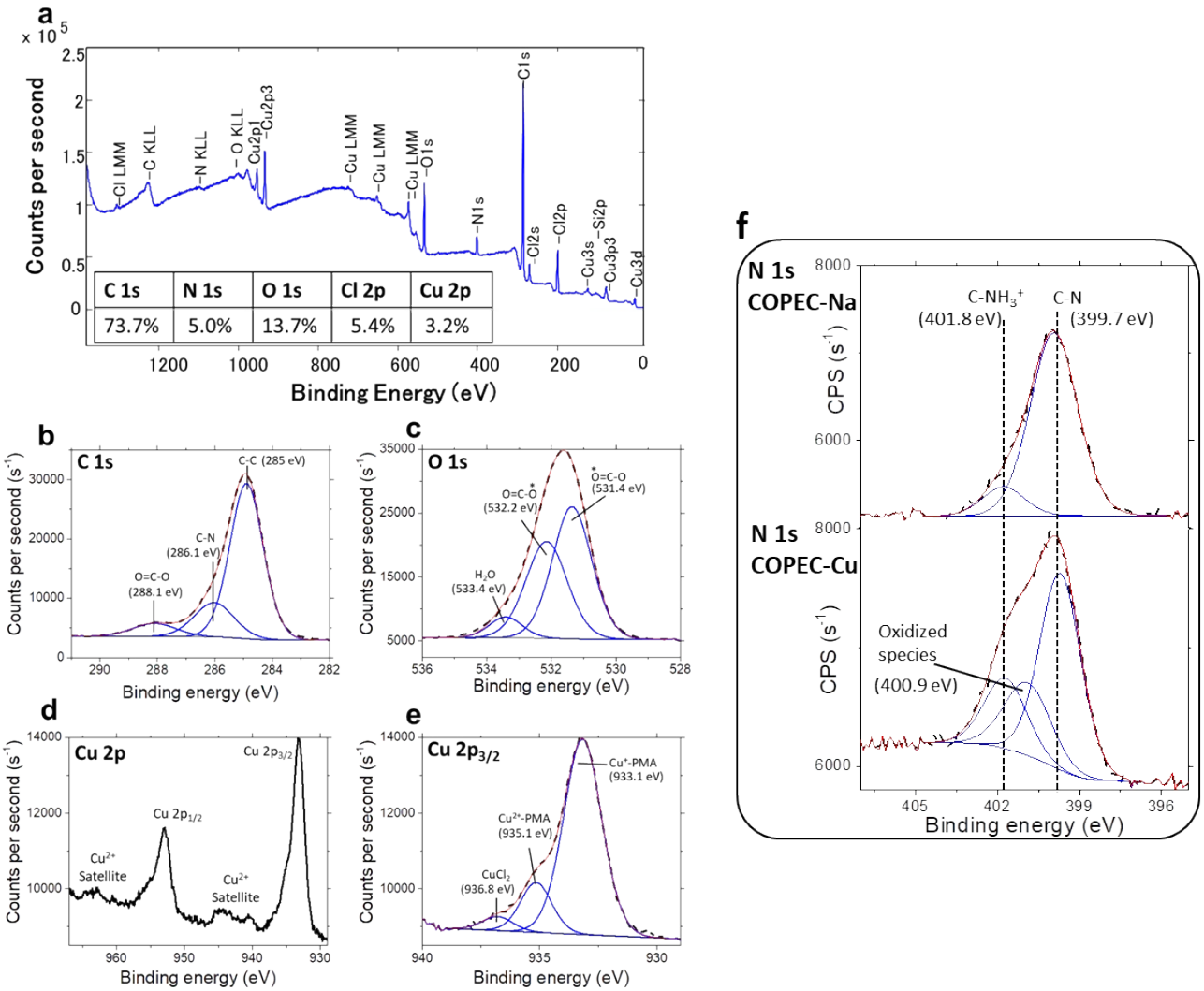

Fig. S2: XPS atomic survey (a), corresponding atomic abundancy table and peaks deconvolutions (b,c,d,e) of PMAA/PAH COPEC after incubation with a 0.2 M $CuCl_2$ solution at pH 3 for 600 min. (f) Peak deconvolution of high resolution spectra of N1s in COPECs before (Na) and after (Cu) incubation with $CuCl_2$.

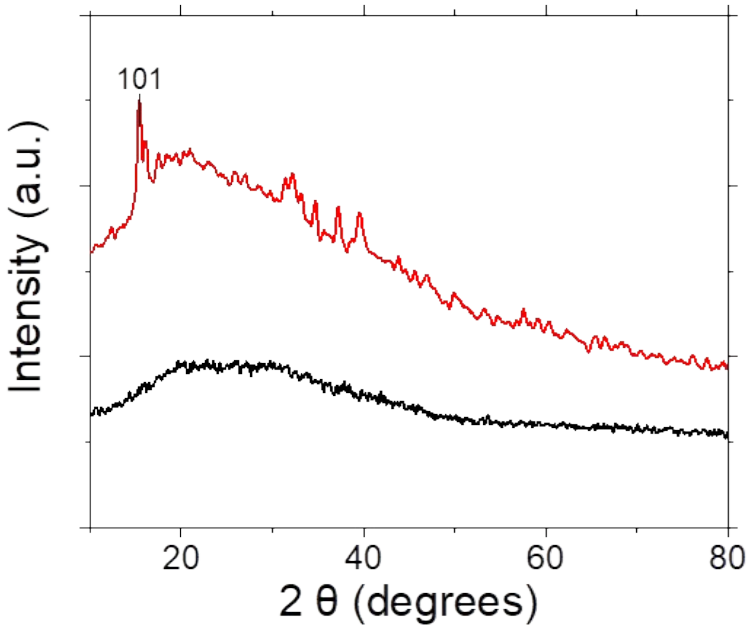

Fig. S3: Typical XRD diffraction patterns of dried PMAA/PAH COPECs before (black line) and after (red line) incubation in 0.2M $CuCl_2$ for 600 min at pH 3.

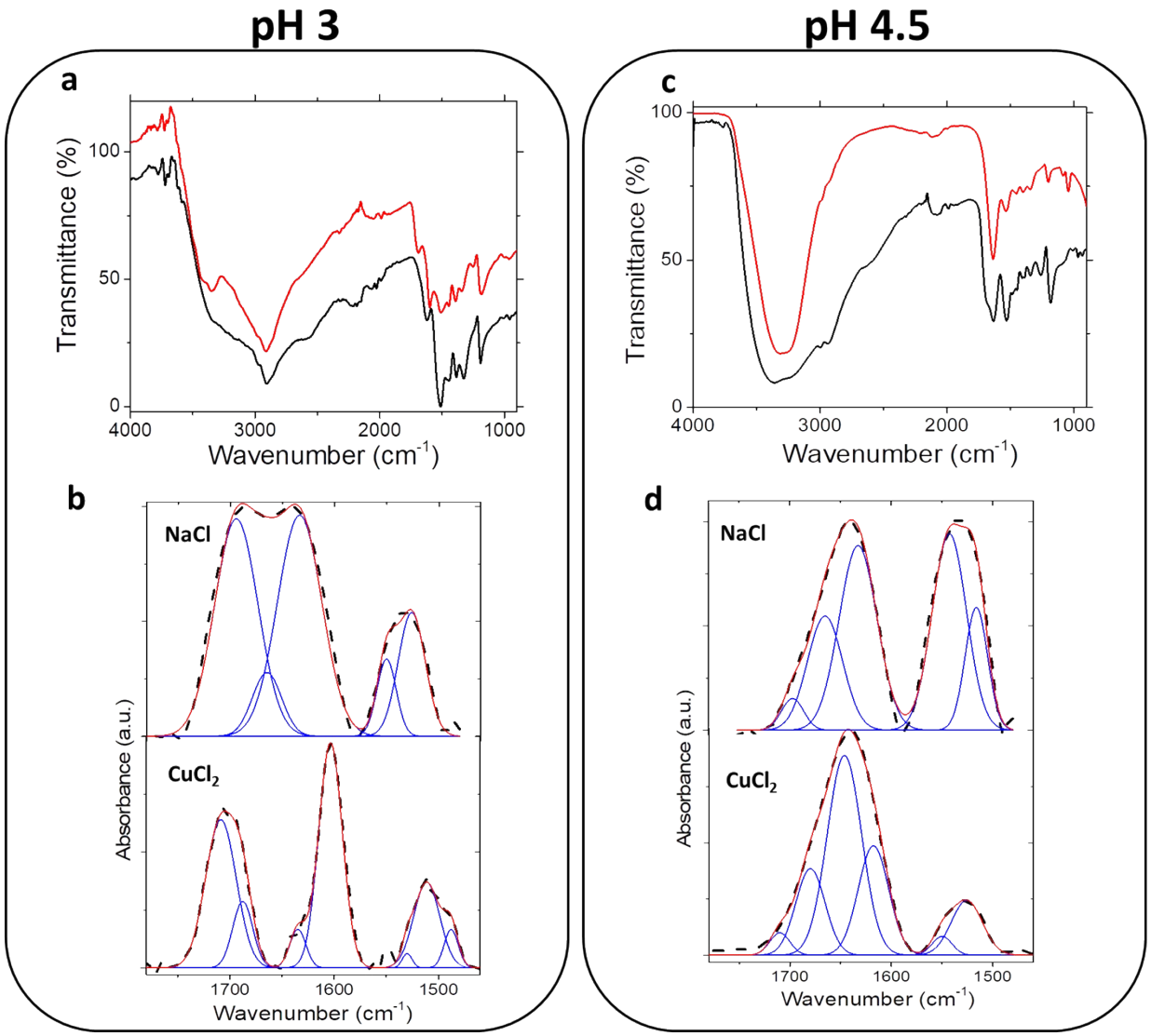

Fig. S4: ATR-FTIR spectra of PMAA/PAH COPEC after incubation with a 0.2 M $CuCl_2$ solution for 600 min at pH 3 (a) and pH 4.5 (c). Deconvoluted ATR-FTIR signal (red line) and experimental data (black dotted line) from PMAA/PAH COPECs incubated at pH 3 (b) and 4.5 (d) in the region from 1450 cm^{-1} to 1780 cm^{-1}.

Assignment	Peak	COPEC	COPEC Cu
O-H (s) H-bonded	3500-3000	X	
N-H (s)	3430-3360		X
N-H (s)	3370		
C-H (s)	2980 2923	X	X
C=O (s) C=O associated (s)	1697 1664	X X	X (1708) X (1679)
COO^--Cu bridging (s)	1615		X
N-H (bending)	1631	X	X(1645)
COO- (a.s)	1542	X	X(1548)
N-H (scissor)	1516	X	X(1521)
C-H_3 (b)	1470-1450	X	X
C-O-H (b)	1440-1390-1394	X	X
	1384	X	
C-O and C-N (s)	1340		X
	1320	X	
	1310		
	1250	X	X
	1180-90 (broad)	X	X
C-N (s)	1200-1000	X	X
O-H (b)	960	X	X
C-H (b)	935	X	X
C-H (b)	Around 860	840	857
C-H (b)	Around 770	765	765

Table S1: Peak attribution from ATR-FTIR spectra of PMAA/PAH COPEC before and after incubation in 0.2M $CuCl_2$ solutions at pH 3 and pH 4.5**.**

	pH 3	pH 3 Cu	pH 4.5	pH 4.5 Cu
COOH	1698 A = 2467	1707 A=2535	1697 A=210	1708 A=240
COOH associated	1660 A= 487	1685 A=691	1664 A=1184	1679 A=1202
NH_3	1620	1634	1631	1645
COO-Cu	-	1605 A=2636	-	1615 A=1940
COO^-	1545 A= 475	1538 A=74.1	1542 A=1792	1548 A=204
NH_3	1510	1511	1516	1521

Table S2: Attribution and respective areas of contribution components to the ATR-FTIR spectrum of PMAA/PAH COPECs before and after incubation. Areas were used for calculating the carboxylate deprotonation rate and its bridging complexation rate in COPECs.

Calculation of the deprotonation rate of PMAA from ATR-FTIR deconvolution areas:

In the case of the PMAA/PAH COPEC:

$$D_{PMAA}^{pH}(\%) = \frac{A_{COO^-}^{pH}}{A_{COO^-}^{pH} + A_{COO^-(associated)}^{pH} + A_{COOH}^{pH}} \times 100$$

In the case of the PMAA/PAH COPEC after incubation in $CuCl_2$:

$$D_{PMAA}^{pH}(\%) = \frac{A_{COO^-}^{pH} + A_{COO-Cu}^{pH}}{A_{COO^-}^{pH} + A_{COO-Cu}^{pH} + A_{COO^-(associated)}^{pH} + A_{COOH}^{pH}} \times 100$$

Calculation of the bridging complexation rate of carboxylate groups with copper ions:

$$C_{bridging}^{pH}(\%) = \frac{A_{COO-Cu}^{pH}}{A_{COO^-}^{pH} + A_{COO-Cu}^{pH}} \times 100$$

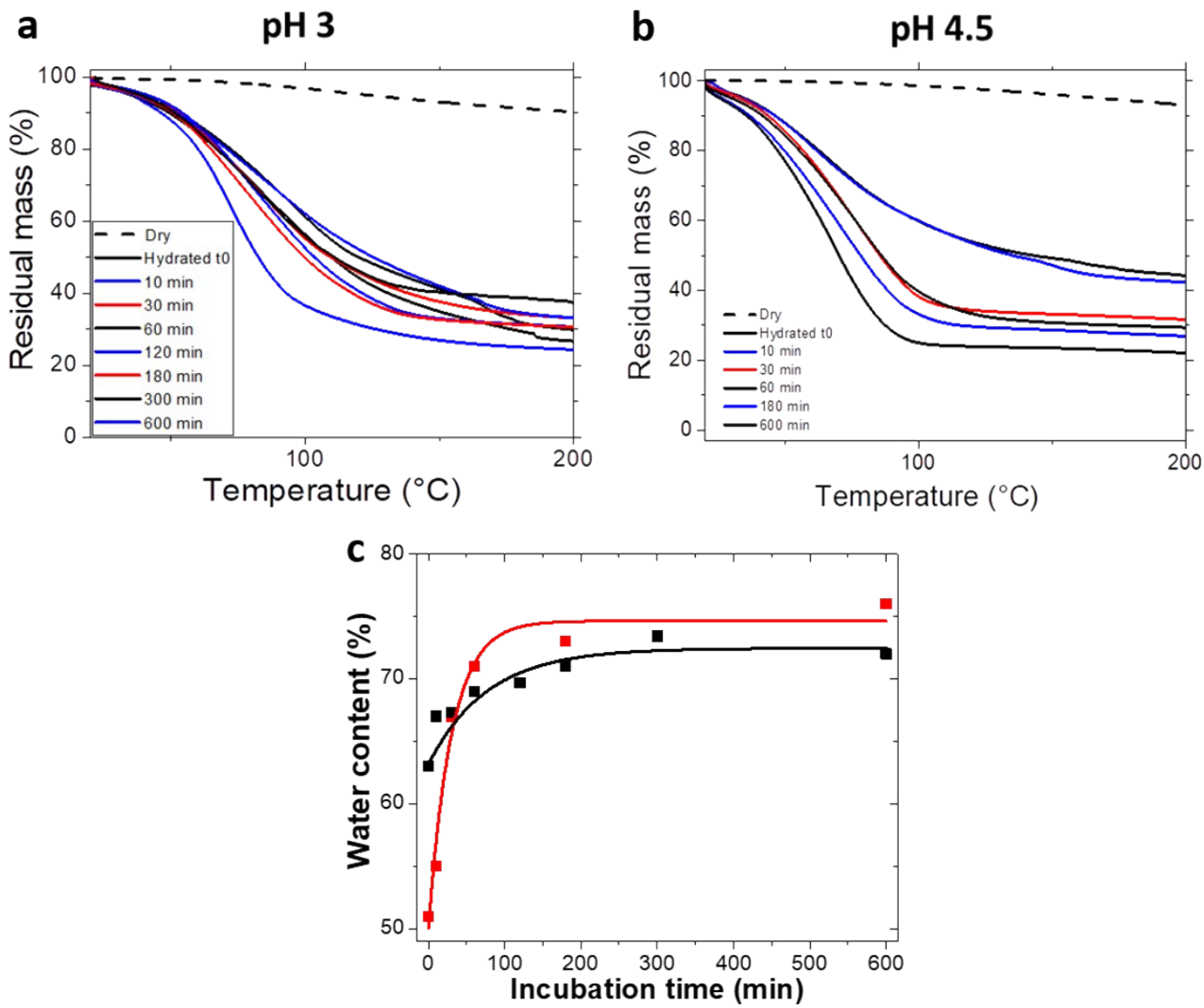

Fig. S5: Thermogravimetric analysis of PMAA/PAH COPECs and water content. TGA analysis of PMAA/PAH COPEC at increasing incubation times from 0 to 600 min in a 0.2 M $CuCl_2$ solution at pH 3 (a) and pH 4.5 (b). Evolution of the water content of PMAA/PAH COPECs as a function of the incubation time in a 0.2 M solution of $CuCl_2$ (c) at pH 3 (black line) and pH 4.5 (red line). The water content was determined at 180 °C by subtracting the mass losses of the COPEC in the dry state and at the considered incubation time. COPECs were first equilibrated at the considered pH in a 0.6 M NaCl before performing incubation in $CuCl_2$ solutions. Data were plotted by using the equation $y = a + be^{-t/t_1}$

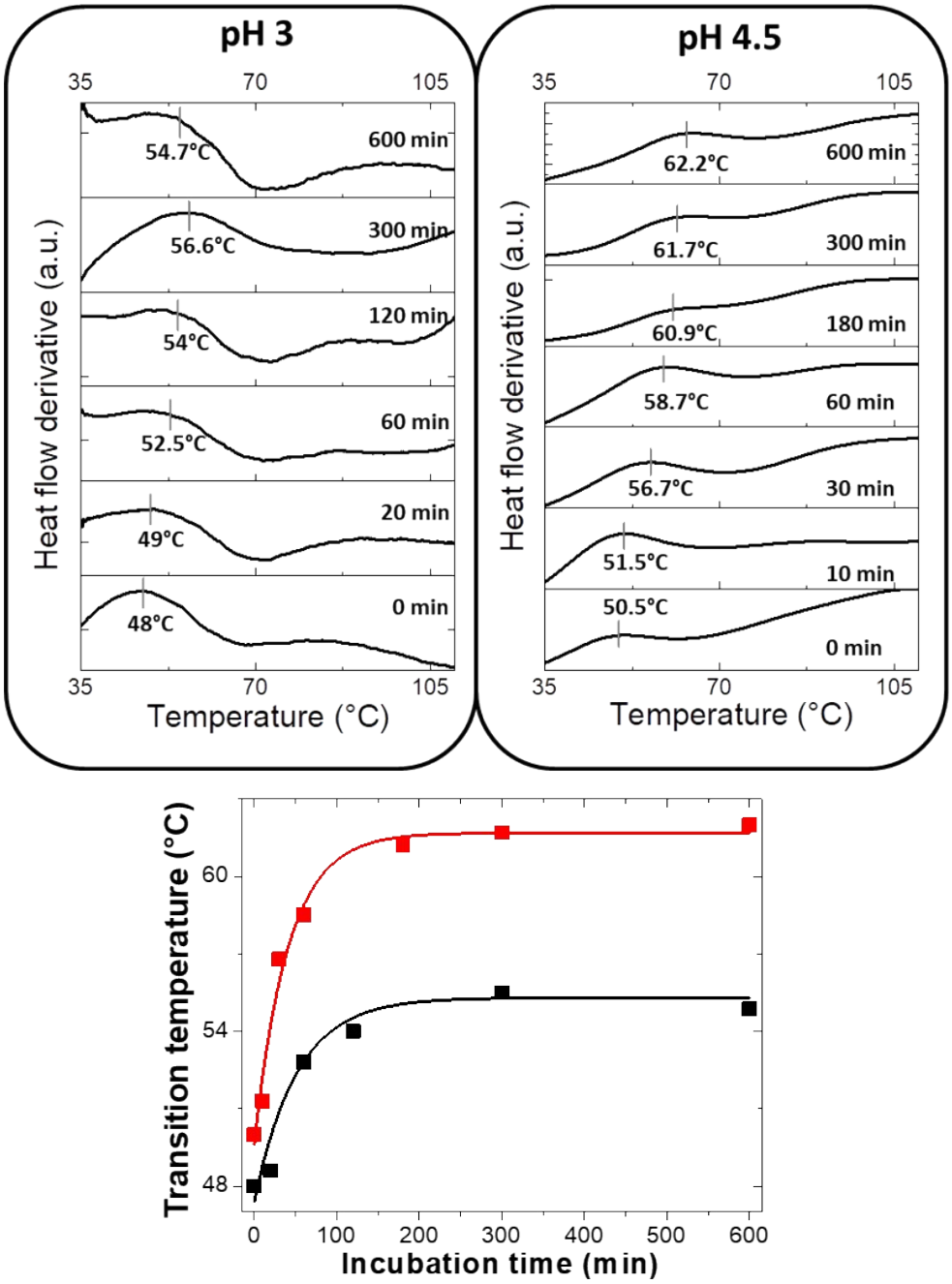

Fig. S6: Differential scanning calorimetry analysis of of PMAA/PAH COPECs and transition temperature. Second derivative of the second scan of DSC analysis of dry PMAA/PAH COPECs at increasing incubation times from 0 to 600 min in 0.2 M $CuCl_2$ solutions at pH 3 and pH 4.5. Evolution of the transition temperature of PMAA/PAH COPECs as a function of the incubation time in a 0.2 M solution of $CuCl_2$ at pH 3 (black line) and pH 4.5 (red line). COPECs were first equilibrated at the considered pH in a 0.6 M NaCl before performing incubation in $CuCl_2$ solutions. Data were plotted by using the equation $y = a + be^{-t/t_1}$.

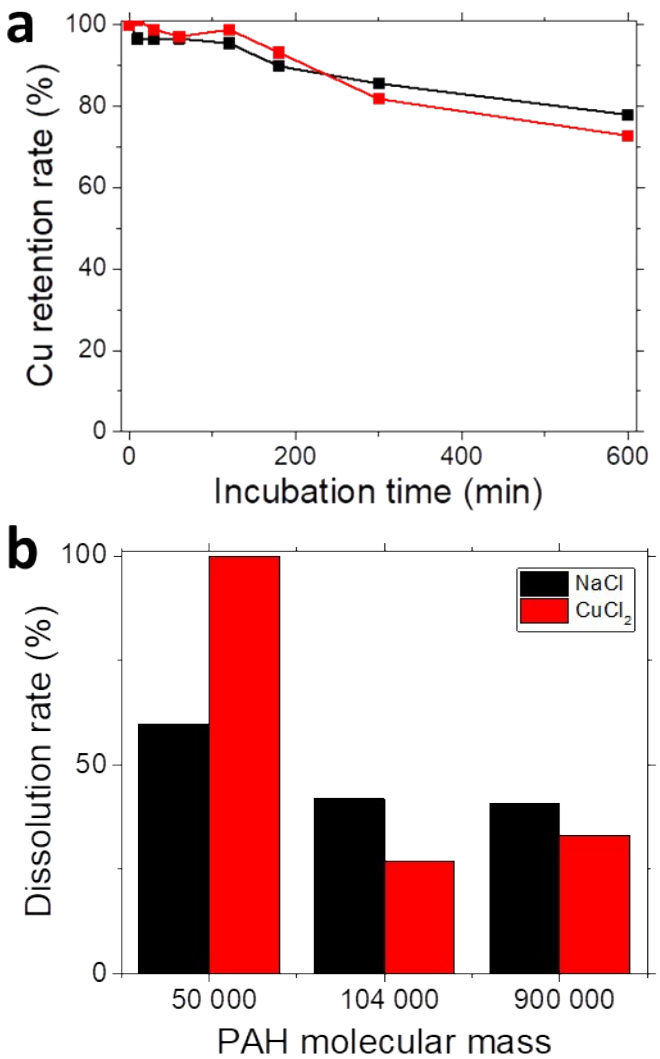

Fig. S7: (a) Retention rate of copper ions in Cu-incubated COPECs upon exposure to a 0.6M NaCl solution at pH 3 (black line) and pH 4.5 (red line). The rate was calculated from ICP analysis as : $R(\%) = \frac{M_{NaCl}^{pH,\,t}(Cu)}{M_{CuCl2}^{pH,\,600}(Cu)}.100$. (b) Dissolution rate of COPECs (black bars) and Cu-Incubated COPECs (red bars) after 200 min incubation in a 2M NaCl solution at 50°C. and pH 3. The rate was calculated from COPEC masses as: $D(\%) = \frac{m(t0) - m(t)}{m(t0)}.100$

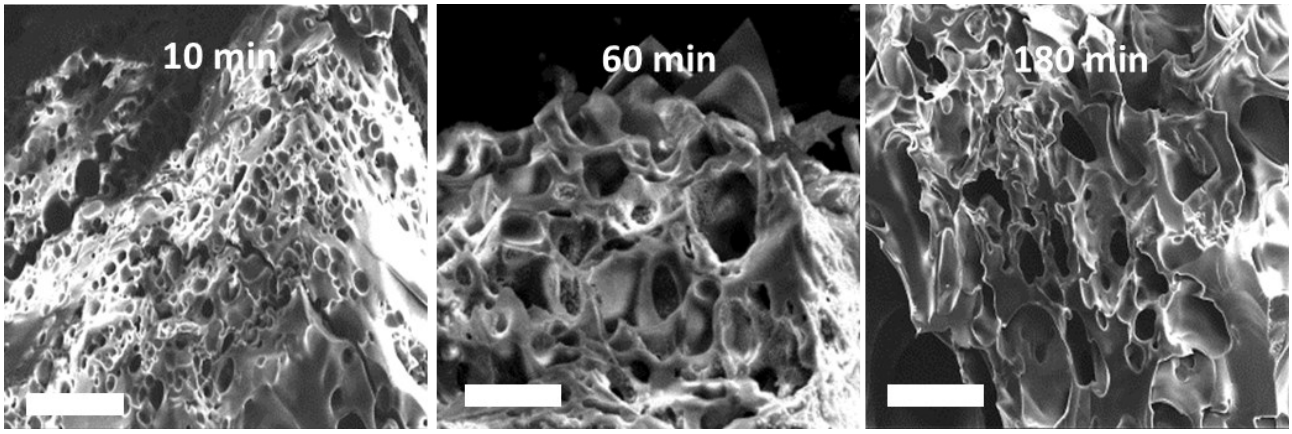

Fig. S8: Structural changes during cation exchanges. Typical SEM micrographs of the cross-sectional view of PMAA/PAH COPECs after incubation from 10, 60 and 180 min in a 0.2 M $CuCl_2$ solution at pH 4,5. Scale bars represent 50 µm.

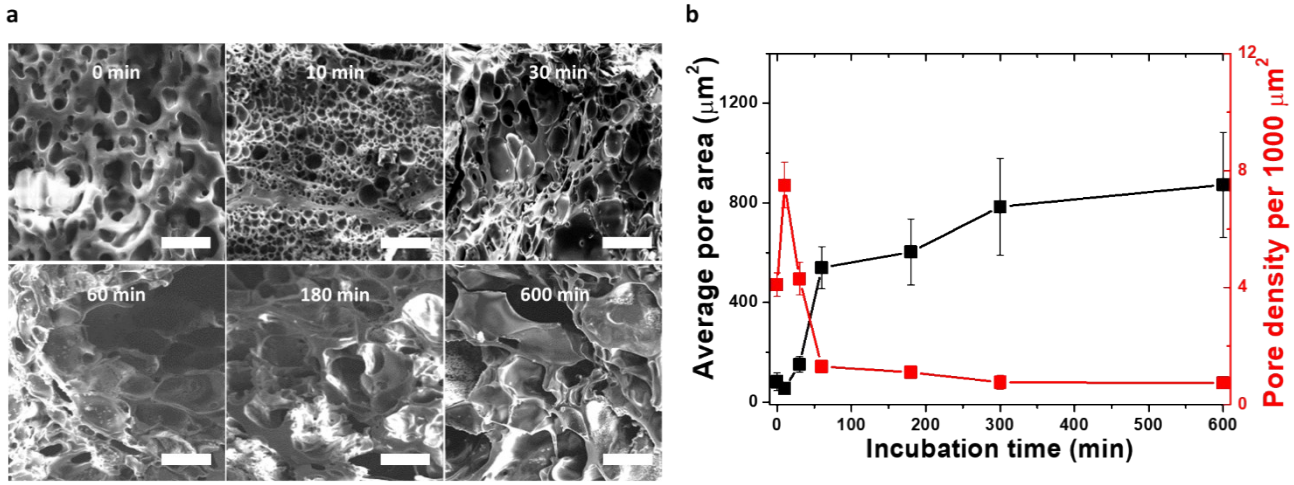

Fig. S9: Structural changes during cation exchanges. Typical SEM micrographs (a) of the cross-sectional view of PMAA/PAH COPECs after incubation from 0, 10, 30, 60, 180 and 600 min in a 0.2 M $CuCl_2$ solution at pH 4,5. Corresponding evolution of the average pore area (black line) and pore density (red line) as a function of the incubation time (b), obtained by software analysis of the micrographs. Scale bars represent 50µm.

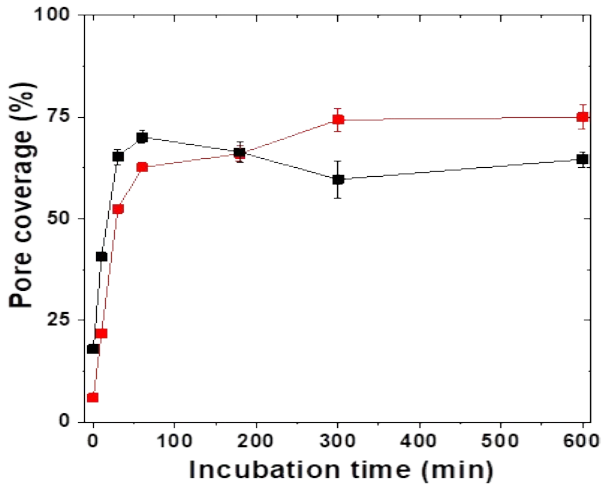

Fig. S10: Pore coverage (%) calculated by using the ImageJ software on SEM micrographs of PMAA/PAH COPECs at increasing incubation times from 0 to 600 min in a 0.2 M $CuCl_2$ solution at pH 3 (black line) and pH 4.5 (red line).

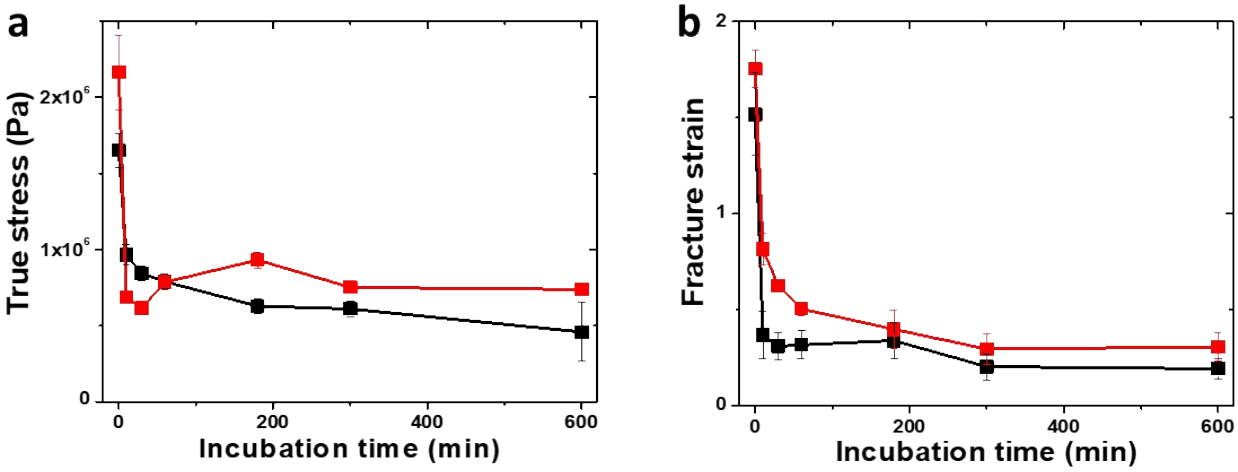

Fig. S11: Evolution of the true stress (a) and fracture strain (b) of PMAA/PAH COPECs, calculated from strain-to-break measurements, at increasing incubation times in a 0.2 M $CuCl_2$ solution at pH 3 (black line) and pH 4.5 (red line).

Amplitude and Kinetics of the COPEC response to cation exchange.

Both the amplitude and the kinetics of the COPEC responses were studied at pH 3 and pH 4.5 during the incubation with 0.2 M $CuCl_2$ solutions. Comparisons were made between water content, pore coverage, elastic modulus, transition temperature and toughness of the incubated COPECs (Fig. S10a). For all these parameters, saloplastics incubated at pH 4.5 exhibited a more intense response as compared to those incubated at pH 3. This trend reflects the significance of the initial molecular and macromolecular configuration to predict the amplitude of the saloplastic's response to stimuli. At higher pH, PMAA/PAH COPECs typically present a higher density of intrinsic PMAA/PAH crosslinks points and of extrinsic charge compensation sites. Therefore, this configuration offers a larger potential for variation of the complexation and chain conformation of PMAA and PAH upon incubation with $CuCl_2$ (Fig. S10a). From kinetic aspects, all investigated parameters followed an apparent first-order kinetic that could be fitted with the equation $y = a + be^{-t/t_1}$. Their corresponding characteristic half-life time constants τ (min) were calculated (Table in Fig. S10). At both considered pH, a faster relaxation kinetic was found for larger-scale properties such as the microscopic structure and toughness of COPECs, reaching τ values ranging from 9.9 min at pH 3 to 25.9 min at pH 4.5 (Fig. S10b). The processes associated with polymer chain conformation changes followed a kinetic with characteristic time constants around 30-35 min. The cation exchange was the slowest process to complete

Parameter measured	Characteristic half-life time τ (min)	
	pH 3	pH 4.5
Cu^{2+} intake	49.5	-
Na^{+} release	41.8	40.2
Pore coverage	9.9	25.9
Water content	10.3	24.7
Transition temperature	35.7	32.8
Elastic modulus	29.6	28.3
Toughness	10.0	25.3

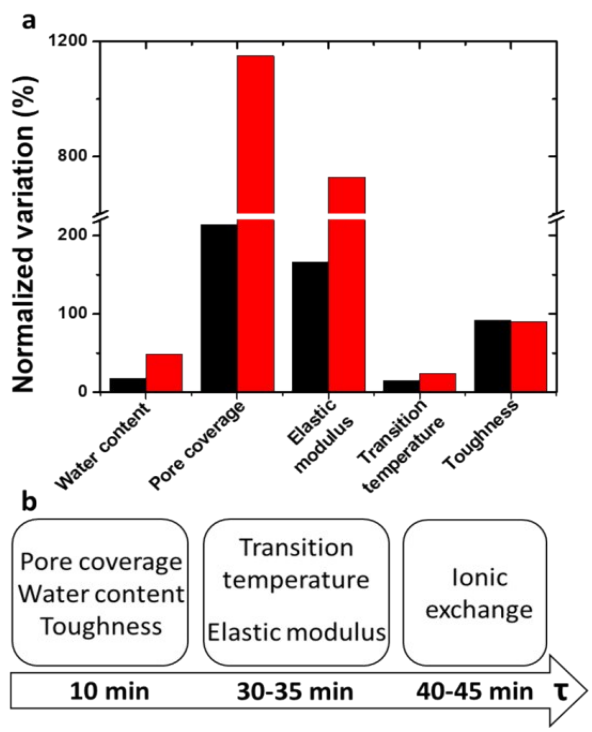

Fig. S12: Variations of incubated PMAA/PAH COPECs properties and their characteristic time τ. Characteristic time constant τ (min) associated with the evolution of each parameter during incubation of PMAA/PAH COPECs with a 0.2 M $CuCl_2$ solution at pH 3 and 4.5. The evolution of each parameter was fitted iteratively with the equation $y = a + be^{-t/t_1}$, until a Chi-Square tolerance value of $1E^{-9}$ was reached. Halftime constant τ was calculated as $\tau = t_1.ln(2)$. (a) Normalized variation (%) associated with the evolution of each parameter before and after incubation of PMAA/PAH COPECs for 10h with a 0.2 M $CuCl_2$ solution at pH 3 (black bars) and 4.5 (red bars). (b) Typical distribution of the characteristic time constant τ (min) associated with the evolution of each parameter during incubation.

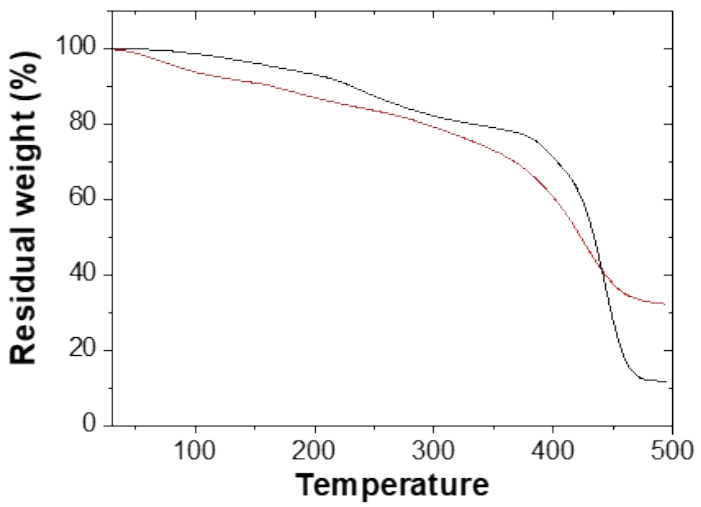

Fig. S13: Thermal Annealing of PMAA/PAH COPEC. TGA analysis of PMAA/PAH COPECs under argon atmosphere before (black line) and after incubation for 600 min in a 0.2 M CuCl (red line).

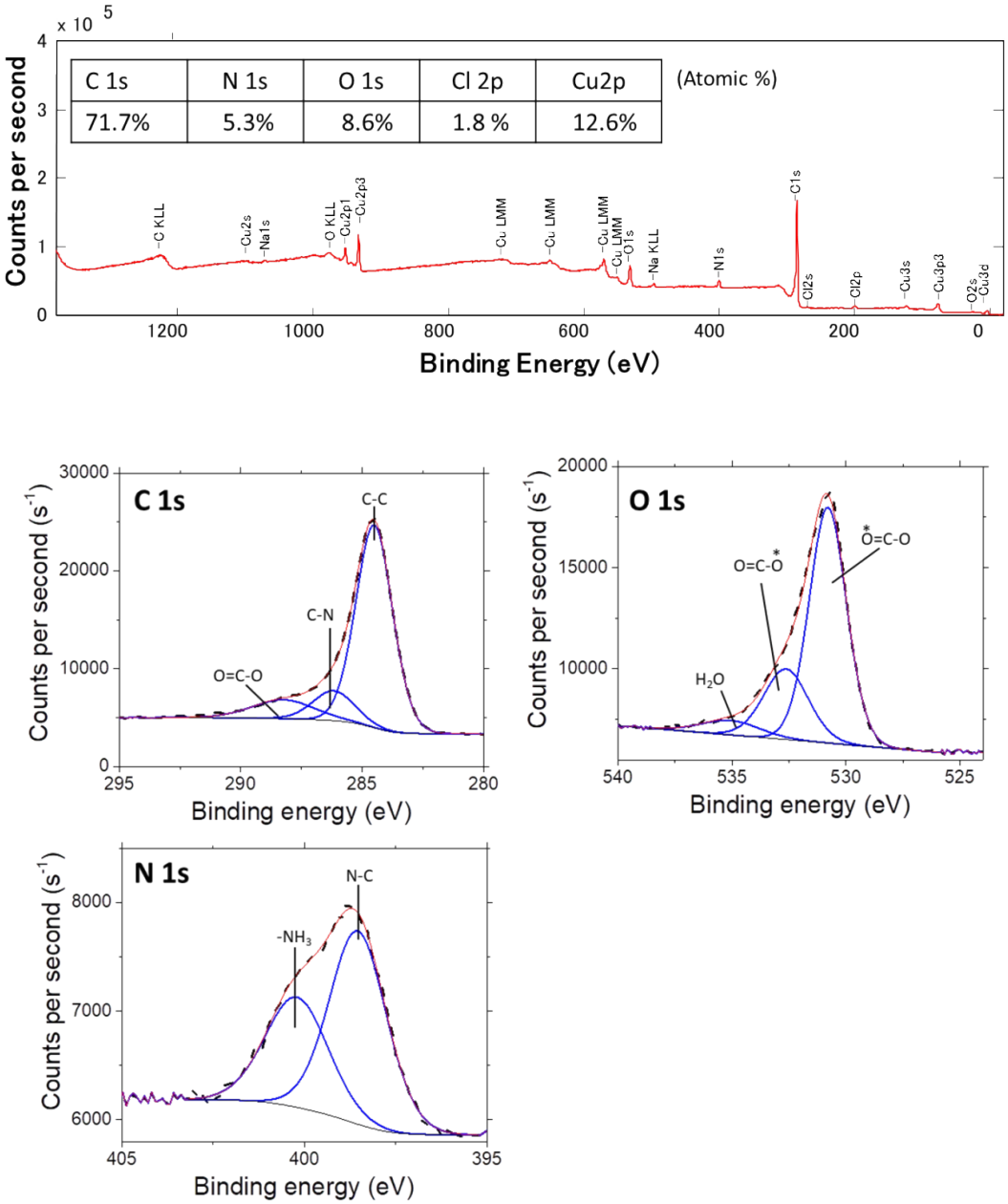

Fig. S14: XPS atomic survey, corresponding atomic abundancy table and peaks deconvolutions of $CuCl_2$ incubated PMAA/PAH COPECs after annealing.

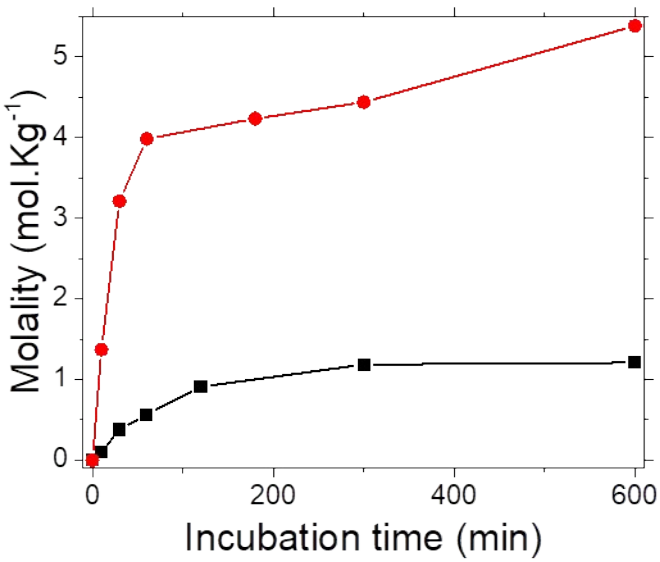

Fig. S15: Molality of copper, measured by ICP, in dry PMAA/PAH COPECs before (black line) and after (red line) annealing. PMAA/PAH COPEC were incubated with a 0.2 M $CuCl_2$ solution at pH 4.5 for increasing times, then vacuum dried and annealed at 500 °C under argon.

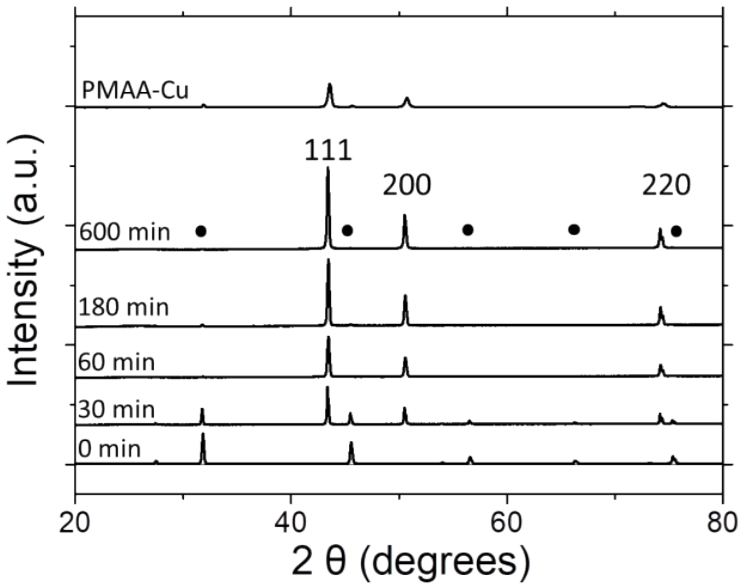

Fig. S16: XRD of annealed PMAA/PAH COPECs. Typical XRD diffraction patterns of PMAA/PAH COPECs and PMAA-Cu after annealing at 500°C under argon and initially incubated in a 0.2 M $CuCl_2$ solution at pH 4.5 during 0 to 600 min. The location of initial peaks from NaCl is pointed by black circles.

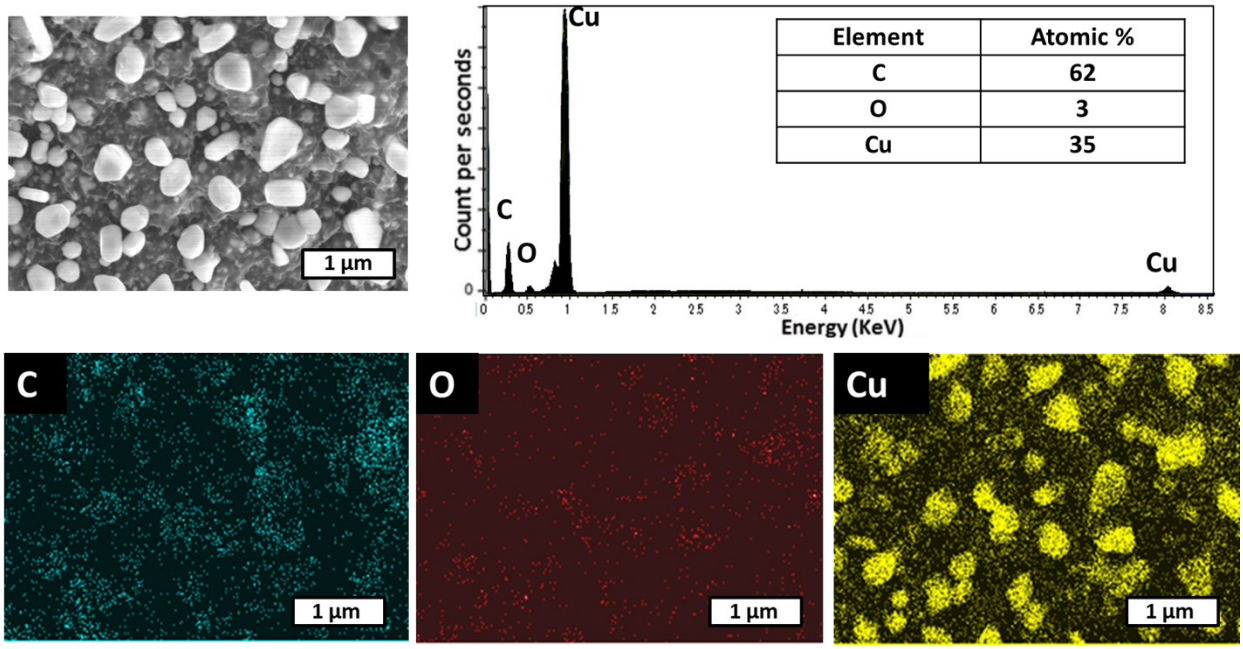

Fig. S17: Elemental mapping of incubated PMAA/PAH COPECs after annealing. Typical SEM micrograph and corresponding EDX analysis of a PMAA/PAH COPEC incubated for 600 min with a 0.2 M $CuCl_2$ solution at pH 4.5 after annealing at 500 °C under argon.

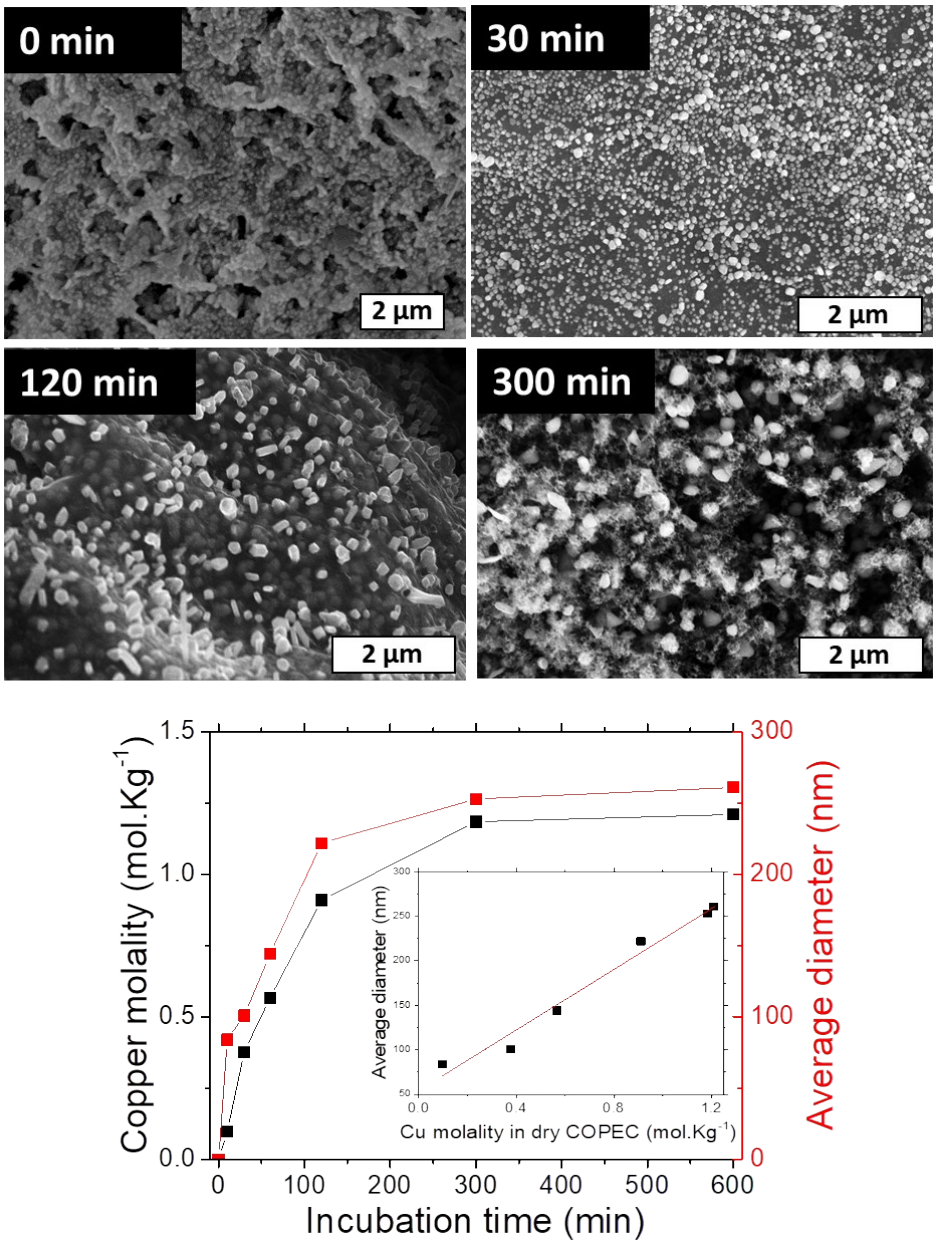

Fig. S18: Growth of copper nanoparticles in PMAA/PAH COPECs in function of incubation time. Typical SEM micrographs of PMAA/PAH COPECs initially incubated in a 0.2 M $CuCl_2$ solution at pH 4.5 during 0 to 300 min after annealing at 500 °C under argon. Corresponding evolution of the copper molality in dry saloplastics before annealing (black line) and of the average diameter of copper nanoparticles formed after annealing (red line) as a function of the incubation time. In inset, evolution of the NP average diameter as a function of the copper molality in dry saloplastics before annealing.

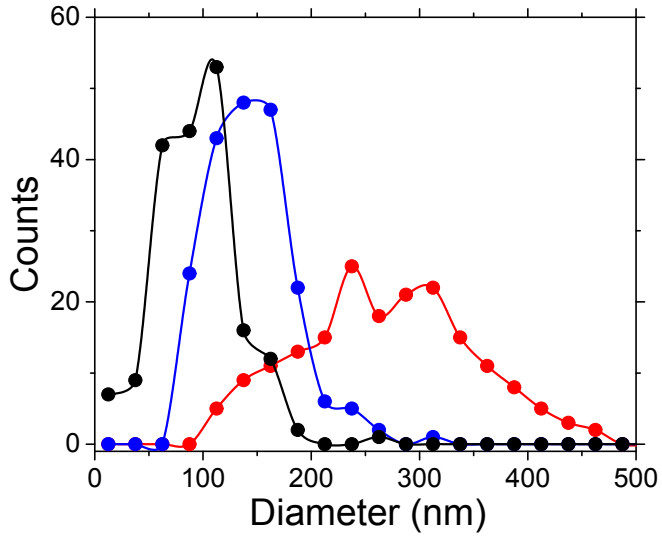

Fig. S19: Calculated size distribution of copper nanoparticles in PMAA/PAH COPECs after annealing of saloplastics initially incubated in a 0.2 M $CuCl_2$ solution at pH 4.5 during 10 min (black line), 60 min (blue line) and 600 min (red line).

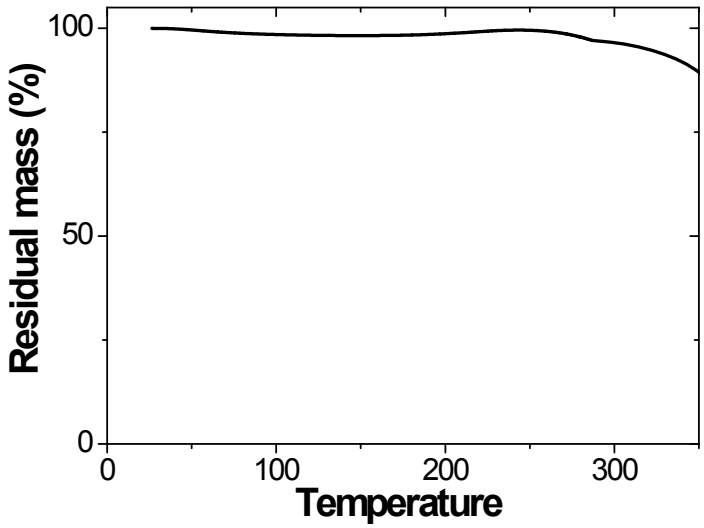

Fig. S20: TGA analysis of PMAA/PAH COPEC under air, after previous annealing at 500 °C under argon.

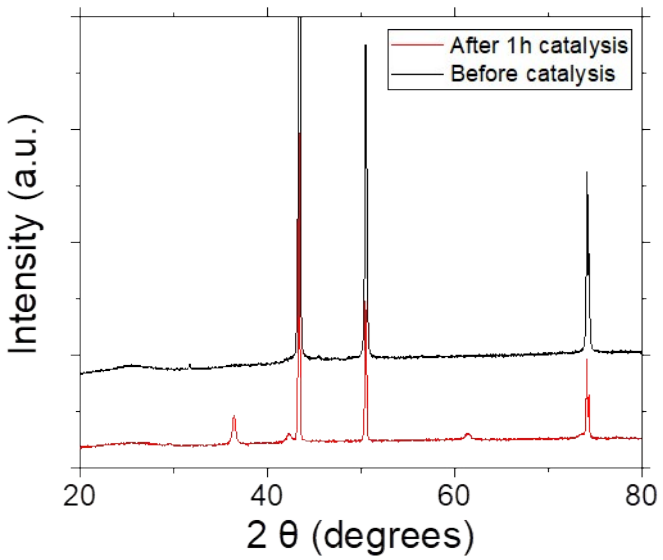

Fig. S21: Typical XRD diffraction patterns of annealed Cu-incubated PMAA/PAH COPECs before (black line) and after (red line) being used as catalyst for CO oxidation at 300°C for 60 min.

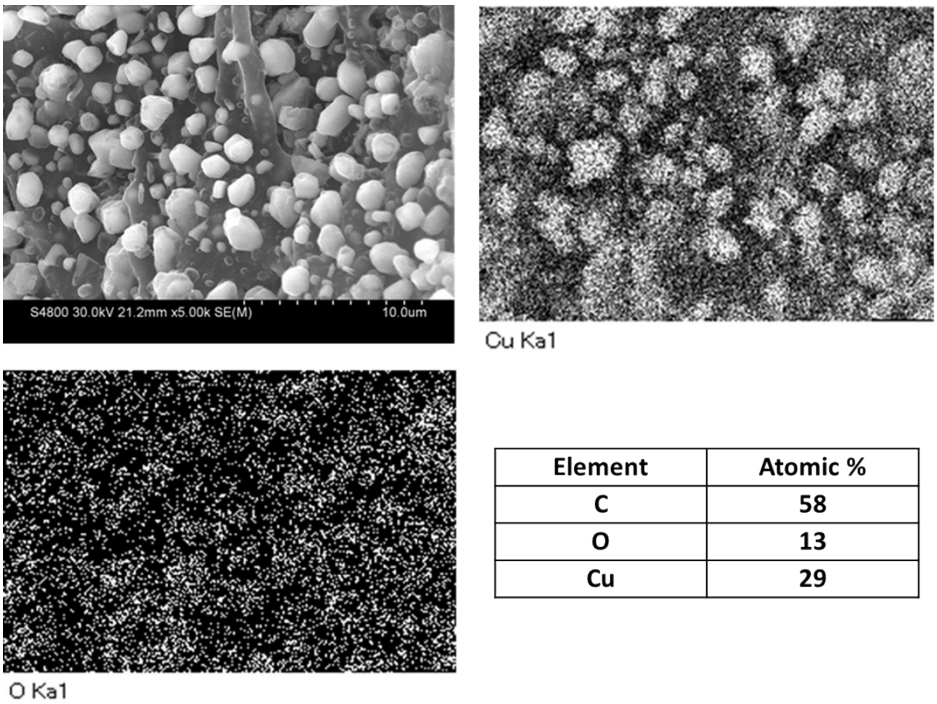

Element	Atomic %
C	58
O	13
Cu	29

Fig. S22: Elemental mapping of incubated copper-loaded PMAA/PAH COPECs after a catalysis cycle. Typical SEM micrograph and corresponding EDX analysis of copper-loaded PMAA/PAH COPECs after a catalysis cycle at 300 °C under O_2 and CO conditions.

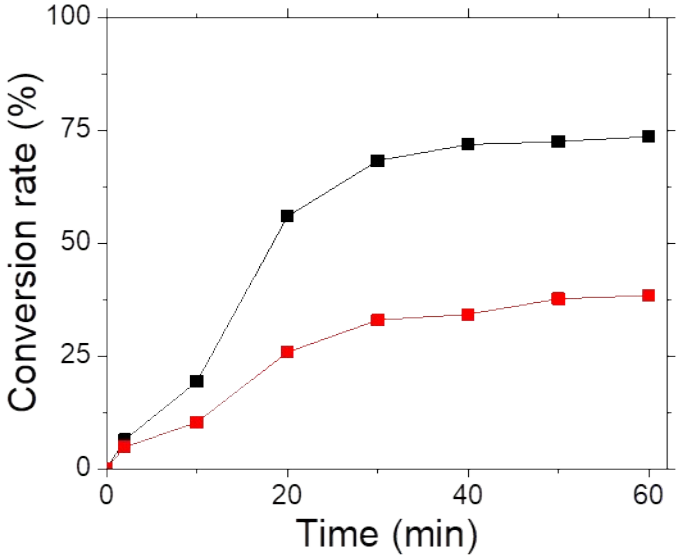

Fig. S23: Conversion rate (%) of CO oxidation in function of contact time with 10 mg of annealed COPEC previously incubated for 300 min during the first (black line) and the second (red line) catalysis cycle.

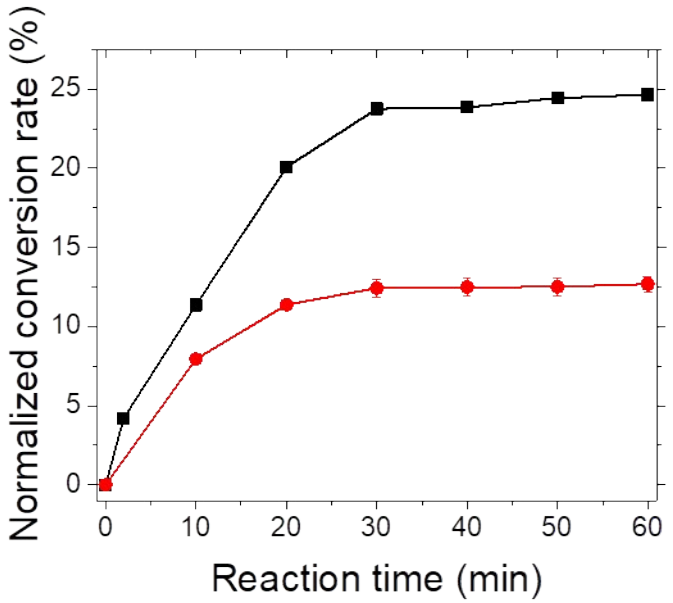

Fig. S24: Conversion rate normalized by the copper content (%.mg^{-1}) of CO oxidation in function of contact time with 10 mg of annealed COPEC previously incubated for 300 min (black line) and commercial copper nano-powder (red line).